Bioconjugate Chemistry

Article

pubs.acs.org/bc

Confined Singlet Oxygen in Mesoporous Silica Nanoparticles: Selective Photochemical Oxidation of Small Molecules in Living Cells

Takuma Nakamura,[†] Aoi Son,[†] Yui Umehara,[†] Takeo Ito,[†] Ryohsuke Kurihara,[‡] Yuta Ikemura,[‡] and Kazuhito Tanabe*[,‡]

[†]Department of Energy and Hydrocarbon Chemistry, Graduate School of Engineering, Kyoto University, Nishikyo-ku, Kyoto, 615-8510, Japan

[‡]Department of Chemistry and Biological Science, College of Science and Engineering, Aoyama Gakuin University, 5-10-1 Fuchinobe, Chuo-ku, Sagamihara, 252-5258, Japan

Supporting Information

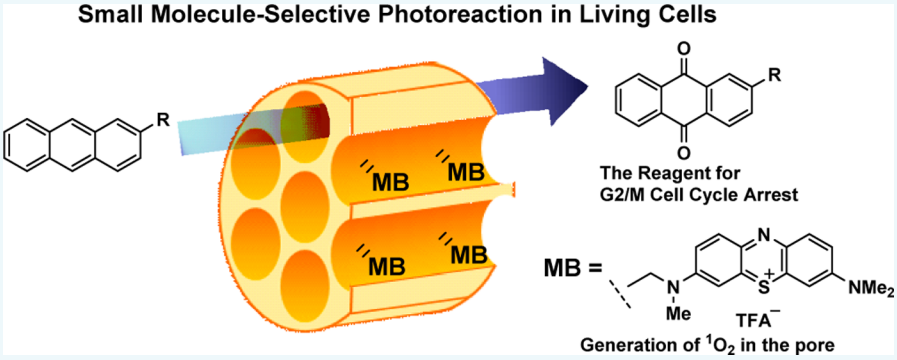

ABSTRACT: Chemical conversion of specific bioactive molecules by external stimuli in living cells is a powerful noninvasive tool for clarification of biomolecular interactions and to control cellular functions. However, in chaotic biological environments, it has been difficult to induce arbitrary photochemical reactions on specific molecules because of their poor molecular selectivity. Here we report a selective and nontoxic photochemical reaction system utilizing photoactivated mesoporous silica nanoparticles to control biological functions. Methylene blue modification within nanoparticle pores for photosensitization produced singlet oxygen confined to the pore that could mediate selective oxidation of small molecules without any damage to living cells. This intracellular photochemical system produced bioactive molecules in situ and remotely controlled the cell cycle phase. We also confirmed that this photoreaction could be applied to control cell cycle phase in tumor tissue transplanted in mice. The cell cycle phase in the cells in mice, to which our system was administered, was arrested at the G2/M phase upon photoirradiation. We demonstrate a simple and promising method for the exogenous conversion of an intracellular biomolecule to another functional compound.

INTRODUCTION

Noninvasive remote control of cellular functions has attracted considerable attention.[1−4] Since the identification of cellular functions is directly linked to the comprehension of life phenomenon, drug design, and medical treatment, there are increasing demands for the development of systems to regulate their functions. In the past, various attempts have been made to manipulate cellular functions using external stimuli. One of the most valuable technologies for remote control of cellular functions is the application of photoirradiation.[5−9] Because of its capability for spatial and temporal control of chemical reactions, this technique has been widely applied to biological experiments. Nevertheless, it has been difficult to implement molecule-specific photoreactions in living cells for the following reasons. First, the complexity of the chaotic environment of the cells, which consists of numerous biomolecules ranging from small molecules to biopolymers such as nucleic acids and proteins, makes it difficult to excite specified molecules, which interact with particular ones, even under irradiation conditions using selected wavelength. The second problem is the generation of reactive oxygen species (ROS) including singlet oxygen ($^1O_2$) that are formed from interactions between triplet-excited-state molecules and molecular oxygen in the ground state.[10−13] ROS have been used for photodynamic therapy (PDT), but ROS oxidizes biomolecules widely to damage living cells and tissue. Therefore, ROS potentially cause serious side effects as well as beneficial effects. These two barriers have limited the broad application of photochemical reactions to biological experiments designed to understand and regulate the functions of living cells and organisms.

Received: February 1, 2016
Revised: March 23, 2016

DOI: 10.1021/acs.bioconjchem.6b00061
Bioconjugate Chem. XXXX, XXX, XXX−XXX

Scheme 1. Synthesis of MSN-MB from MSN-CO_2H

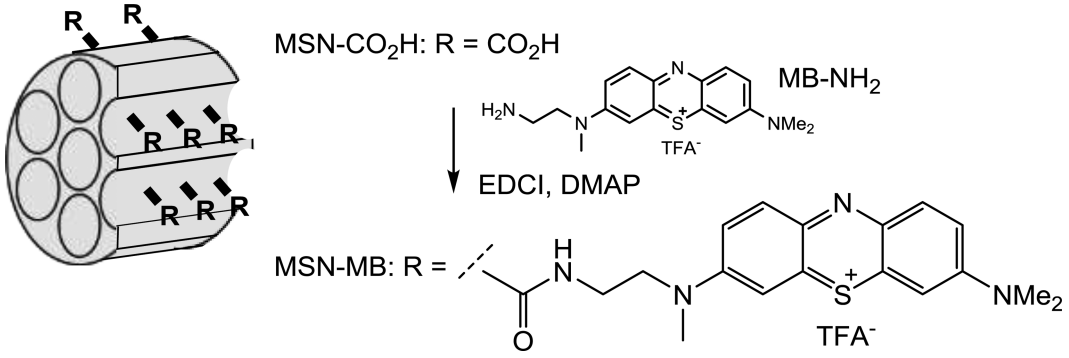

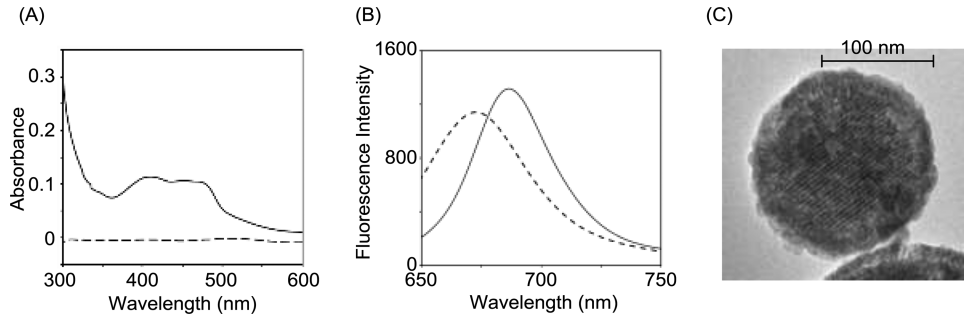

Figure 1. (A) Absorption spectra of MSN-MB (1.0 mg/mL, solid line) and MSN-CO_2H (1.0 mg/mL, dashed line) in DMSO. (B) Fluorescence spectra of MSN-MB (1.0 mg/mL (41 μM of MB units), solid line) and MB-NH_2 (41 μM, dotted line) in DMSO (Ex. 630 nm). (C) TEM image of MSN-MB.

In this study, we attempted to design a photochemical molecular conversion system without any side effects using mesoporous silica nanoparticles (MSN). The pores of the MSN, which were functionalized by chemical modification, provide a limited reaction field for small molecules in living cells, meaning that a highly selective reaction can be implemented. MSN have several favorable features: they are easily fabricated, have a large surface area, have remarkable transparency for a wide range of wavelengths, and provide amorphous frameworks with a large number of silanol groups for postmodification. Heretofore, due to these characteristics, MSN have been widely applied as functional materials such as catalysis[14−17] for photoreaction or organic synthesis, drug carriers,[18−21] or sensing devices.[22]

These excellent properties of MSN prompted us to apply MSN to photoregulation of biological functions. Our hypothesis was as follows: (1) the pores of MSN can be used for selection of small molecules from the complex mixture of biomolecules in living cells; and (2) large biomolecules such as proteins, sugars, and nucleic acids can be prevented by pore size limitations from passing into the pore to approach the reaction fields. Thus, modification of the pores of MSN allows selective reactions on small molecules. We modified the pores of MSN with methylene blue (MB) photosensitizer, which generates singlet oxygen ($^1O_2$) upon photoirradiation. $^1O_2$ generated in the pore immediately oxidizes those molecules, that can enter the pore. On the other hand, unreacted $^1O_2$ becomes inactivated before exiting the pore, and therefore MSN with MB (MSN-MB) can greatly reduce the harmful effects of $^1O_2$. Eventually, we applied these MSN to control cellular functions. By photoirradiation, we successfully converted anthracene derivatives (preAQ) to anthraquinone (AQ), which caused cell cycle arrest without any cytotoxicity.

RESULTS AND DISCUSSION

Fabrication and Characterization of MSN-MB. Initially, we synthesized MSN-MB as shown in Scheme 1. Coupling of carboxylic-functionalized MSN (MSN-CO_2H) with MB derivatives possessing a primary amino group (MB-NH_2) gave the desired nanoparticles, MSN-MB.

To confirm the incorporation of MB units to MSN, we measured the absorption spectra. Monodisperse MSN-MB had a similar spectrum to MB-NH_2 between 300 and 900 nm, while MSN-CO_2H showed no absorption at these wavelengths (Figure 1A). We also measured the fluorescence spectra of MSN-MB (Figure 1B). Compared with MB-NH_2, MSN-MB showed a red-shifted fluorescence emission because of congestion and stabilization of the MB units on the surface of MSN. These results strongly indicate that MB units were densely embedded in the inner pores. Transmission electron microscopy images revealed that the pore structure was maintained even after modification by MB (Figure 1C). The size of MSN-MB and their pore size (φ) were estimated to be 200 ± 60 and 3.5 nm, respectively. In MSN-MB, the MB units were located mainly in the inner pores. The ratio of the inner surface area to the total surface area of the nanoparticles was calculated to be 96% (eq 1 and 2; see Experimental Section). Because a large majority of the carboxylic acid substituents were located in the inner pore, the modification by MB occurred predominantly in these inner pores. The number of MB units incorporated on the surface of MSN was estimated to be 41 nmol/mg.

Cytotoxicity of MSN-MB upon Photoirradiation. An attempt was made to demonstrate the photochemical function of this system using the human lung carcinoma cell line A549. Initially, we assessed the cytotoxic properties of monadelphous MB-NH_2 under photoirradiation conditions, before the

DOI: 10.1021/acs.bioconjchem.6b00061
Bioconjugate Chem. XXXX, XXX, XXX−XXX

evaluation of properties of the MSN-MB. After administration of MB-NH_2 to A549 cells and incubation for 5 h to allow their penetration into the cells, the medium was replaced with fresh medium to avoid undesirable activation of drugs outside the cells. We then exposed A549 cells to photoirradiation. As shown in Figure 2, a negligible cytotoxic effect was observed in

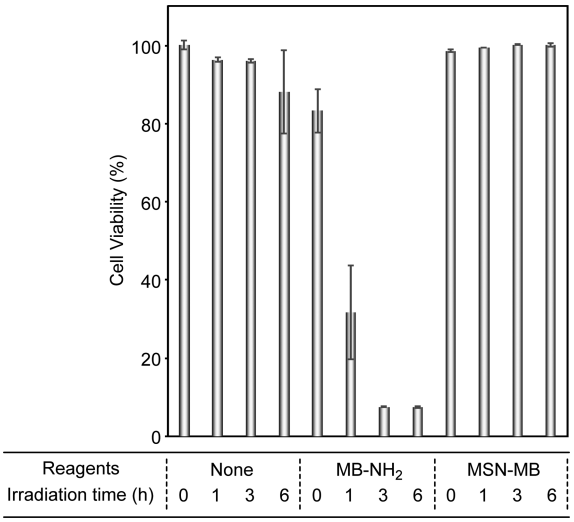

Figure 2. Photoinduced cytotoxicity of MB-NH_2 and MSN-MB against A549 cells. After the cells were incubated for 24 h in the presence or absence of MB-NH_2 (41 μM) or MSN-MB (1.0 mg/mL, 41 μM of MB units in MSN-MB), the cells were irradiated (665 nm, 2.0 mW/cm2) for 0, 1, 3, and 6 h. The cell viability was calculated by means of cell counting kit-8 (WST-8). Results are shown with the mean ± SD (n = 3).

the presence of MB-NH_2 under conditions without photoirradiation. On the other hand, photoirradiation of the cells to which MB-NH_2 was administered resulted in a significant decrease in cell viability, indicating generation of $^1O_2$ by photoirradiation of MB-NH_2. We next conducted similar cellular experiments using MSN-MB, in which the number of MB molecules administered to the cells was equalized to that in cells treated with MB-NH_2 (Figure S1). In contrast to the significant cytotoxic effects of MB-NH_2, MSN-MB showed almost no cytotoxic effect on the cells, even upon photoirradiation. In addition, we estimated the oxidative stress of the cells. We measured the GSH/GSSG ratio in the cells treated with MSN-MB upon photoirradiation. Although the photoirradiation caused slight decrease of the ratio (Figure S2), the change was negligible, indicating that MSN-MB showed less stress on the cells even upon photoirradiation. To elucidate why MSN-MB caused no phototoxicity, we next assessed the generation of $^1O_2$ by means of singlet oxygen sensor green (SOSG), which is a fluorescent indicator of $^1O_2$ (Figure 3A). The cells, to which MSN-MB or MB-NH_2 were administered, were incubated with SOSG for 5 h, and then the cells were photoirradiated for 1 h. We observed a dramatic increase of fluorescence of SOSG from the cells, to which MSN-MB was administered, while negligible increase of emission was observed from the cells incubated without MSN-MB. Thus, the $^1O_2$ was produced in the cells upon photoirradiation, when MSN-MB was administered to the cells, despite the fact that cytotoxicity was undetectable. The experimental result that fluorescence enhancement of SOSG in the presence of MB-NH_2 was lower than that in the presence of MSN-MB suggests

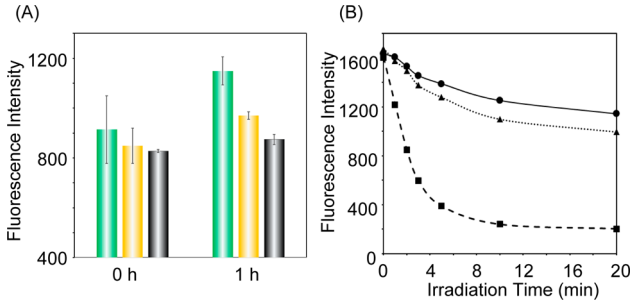

Figure 3. (A) Visualization of singlet oxygen generated in the A549 cells by photoirradiation in the presence of MSN-MB. The fluorescence intensity of SOSG (550 nm) in the cells, in which singlet oxygen was generated by photoirradiation (0 or 1 h) in the presence of MSN-MB (green) or MB-NH_2 (yellow). The fluorescence of SOSG in the absence of photosensitizer was also measured (black). (B) Temporal change of fluorescence intensity of anthracene unit in MSN-Anth. MSN-Anth was photoirradiated (665 nm) in the presence of MSN-MB (0.1 mg/mL, 4.1 μM of MB units in MSN-MB, circle) or MB-NH_2 (4.1 μM, square). The control photoirradiation in the absence of photosensitizer was also conducted (triangle).

that chemical modification of MB-NH_2 by nanoparticles did not interfere with the photochemical generation of $^1O_2$.

To clarify the reason for this suppressed cytotoxic effect, we then evaluated the generation and active area of $^1O_2$ generated inside MSN-MB. First, we measured the quantum yield of $^1O_2$ formation upon photoirradiation of MSN-MB and MB-NH_2. Detection of phosphorescence of $^1O_2$ at 1270 nm revealed that the quantum yield of MSN-MB was estimated to be 0.62, given that the quantum yield obtained from MB-NH_2 was similar to that from methylene blue itself (Φ_Δ = 0.52).[23] Thus, MSN-MB efficiently generated $^1O_2$ under photoirradiation conditions. Second, we estimated the active area of $^1O_2$. Because $^1O_2$ is known to become inactivated in cells within a distance of less than 70 nm,[24,25] we predicted that the active area of $^1O_2$ was limited to the pores of MSN. Active $^1O_2$ was detected by means of anthracene molecules tethered in the pores of MSN (MSN-Anth; see Figure S3), the fluorescence of which was reduced by the [4 + 2] cycloaddition of $^1O_2$.[26,27] Because anthracene units tethered in the pores of MSN-Anth could not enter the pores of MSN-MB, the $^1O_2$ species generated inside the pores of MSN-MB could not react with the anthracene units of MSN-Anth. Therefore, we could track the presence or absence of $^1O_2$ outside the pores of MSN-MB by monitoring the fluorescence of MSN-Anth. We photoirradiated a mixture of MSN-Anth and MSN-MB, and confirmed that the change in fluorescence intensity of the anthracene units was negligible (Figure 3B). In a control reaction, we compared the photoreaction of MB-NH_2 or MSN-MB in the presence of monadelphous 2-aminoanthracene, and confirmed that both photoreactions proceeded immediately (Figure S4). The evidence that the drastic fluorescence decay upon photoirradiation to a mixture consisted of MB-NH_2 and MSN-Anth led to the conclusion that $^1O_2$ was generated mainly within the pores of MSN-MB and was inactivated before leaking out of the pores. Thus, $^1O_2$ species generated in the MSN-MB were confined to the pores, resulting in reduced phototoxicity to living cells even under photoirradiation conditions. We also confirmed that the 2-aminoanthracene was oxidized by MSN-MB under the conditions between pH 5.5 and 7.5; however, the reaction efficiency was lowered probably due to the presence of inorganic salt (Figure S5).

DOI: 10.1021/acs.bioconjchem.6b00061
Bioconjugate Chem. XXXX, XXX, XXX−XXX

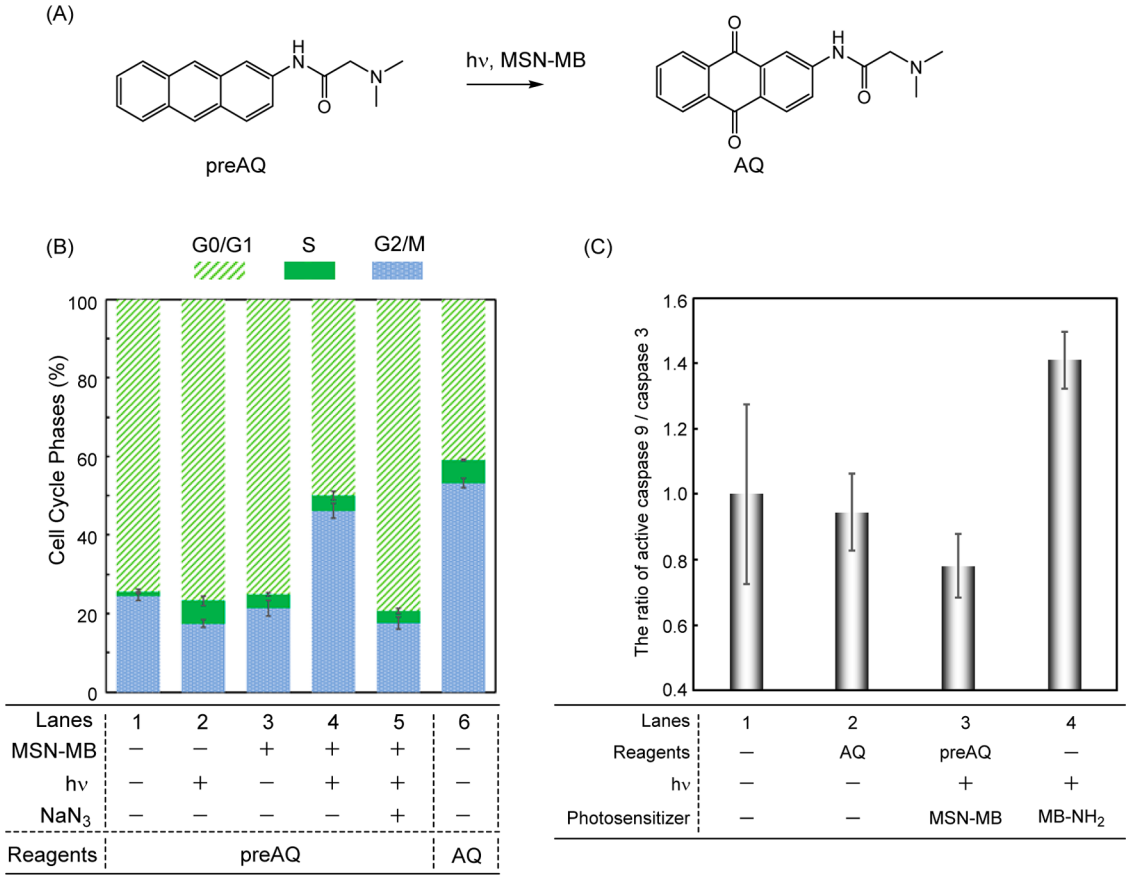

Figure 4. (A) Formation of AQ from preAQ upon photoirradiation in the presence of MSN-MB. (B) Cell cycle phases of A549 cells. The cells were incubated in the presence of designated reagents (preAQ: 10 μM, AQ: 10 μM, NaN_3: 100 μM) and photosensitizer (MSN-MB: 1.0 mg/mL) for 24 h. After wash of the cells, the cells were irradiated (665 nm) for 0 or 3 h and followed by a further incubation for 24 h. The cell cycle phase was analyzed by Nuclear-ID Green Cell Cycle Analysis KIT for flow cytometry. (C) Ratio of active caspase-9 to active caspase-3 in A549 cells, which were treated by AQ, preAQ, MSN-MB, or MB-NH_2 upon photoirradiation (665 nm, 0 or 3 h). After photoirradiation, the cells were further incubated for 72 h and the ratio of active caspases was determined by immunofluorescence detection with APO Logix caspase detection kit.

Remote Photoregulation of the Cell Cycle. We then attempted the remote photoregulation of cellular functions by nontoxic $^1O_2$ generation using the photoreactive MSN-MB system. We chose the cell cycle and its arrest as the target for evaluation of our system. It has been well-documented that anthraquinone derivatives like doxorubicin and daunorubicin induce G2/M cell cycle arrest by intercalation to double-stranded DNA,[28−32] and that they can be synthesized from their corresponding anthracenes by $^1O_2$ oxidation.[33,34] Based on these contexts, we attempted to apply our system for in situ generation of anthraquinone derivatives in the cells to initiate cell cycle arrest (Figure 4). In living cells, preAQ, which has no effect on the cells, would be converted to AQ by photoreaction of MSN-MB without any side effects, and the resulting AQ would lead to arrest of the cell cycle at G2/M phase.

Before the implementation of these cellular experiments, we evaluated the chemical reaction of preAQ in the presence of MB-NH_2 upon photoirradiation by HPLC, and confirmed that preAQ was efficiently converted to AQ (Figure S6). To investigate the induction of G2/M cell cycle arrest by photochemical production of AQ, A549 cells were pretreated with both preAQ and MSN-MB for 24 h and then were photoirradiated (665 nm) for 6 h after washing of the cells to remove the unbound preAQ and MSN-MB. After further incubation for 24 h, the cell cycle was examined using a flow cytometer and a Nuclear-ID Green Cell Cycle Analysis kit. As shown in Figure 4B, the cell cycle phase was not detectably changed compared with nontreated cells when the cells were treated with MSN-MB without photoirradiation. It is striking that photoirradiation of the cells treated with both MSN-MB and preAQ resulted in a remarkable increase in the proportion of cells in the G2/M phase. In separate experiments, we confirmed that addition of NaN_3 as a $^1O_2$ quencher led to the suppression of this change in the cell cycle phase. These results strongly indicate that $^1O_2$ generated in the pores of MSN-MB in the cells reacted with preAQ to form AQ that arrested the cell cycle. It should be noted that no cytotoxicity was observed upon photoirradiation to the cells, which were treated with MSN-MB and preAQ, respectively. Thus, photochemical regulation of the cell cycle was accomplished without any damage to the living cells.

Identification of Photochemical AQ Production in the Cells by Monitoring Caspase-3 and Caspase-9. To clarify whether AQ was produced from preAQ in the cells, we obtained cell extracts and tried to analyze the product. The composition of the lysates was evaluated several times by HPLC; however, identification of AQ production was unsuccessful, probably because the amount of AQ was below the measurable limit. Because we failed to detect the formation of AQ by HPLC, we then attempted the identification of AQ formation using biological methods. We evaluated the activation of caspases, which are a family of cystein proteases

DOI: 10.1021/acs.bioconjchem.6b00061
Bioconjugate Chem. XXXX, XXX, XXX−XXX

that are markers of apoptosis. Recent reports demonstrated that ROS, including $^1O_2$, induce the activation of caspase-9 as well as caspase-3, whereas the cell cycle arrest activates relatively more caspase-3.[35−38] Thus, identification of the species of caspase activation could indirectly verify the generation of AQ leading to cell cycle arrest in the living cells. We evaluated the ratio of active caspase-9 to capase-3 by immunofluorescence detection with an APO Active Detection kit. As shown in Figure 4C, the cells incubated in the presence of MB-NH_2 showed an increase of caspase-9 upon photoirradiation, indicating that $^1O_2$ was effectively generated and induced apoptosis. In the case of the photoreaction system using MSN-MB and preAQ, activation of caspase-3 was greater than that of caspase-9. Control experiments using monadelphous AQ showed that activation of caspase-9 was limited and that caspase-3 was activated slightly, suggesting that photoirradiation of MSN-MB and preAQ generated AQ in the cells, which resulted in arrest of the cell cycle at G2/M phase.

Cell Cycle Arrest in Vivo Experiments. Further attempts were made to demonstrate the in vivo photochemical regulation of cell cycle arrest using the present system. To enhance the biocompatibility of the nanoparticles, polyethylene glycol (PEG)-coated nanoparticles,[24] which had MB units incorporated in their pore (MSN-MB-PEG; see Figure S7) were freshly prepared. For easy handling, we employed tumor tissue as a target to evaluate cell behavior during photochemical treatment. We transplanted colon 26 tumor cells subcutaneously into the lower thigh of nude mice. After the tumor grew to an appropriate size, a solution of preAQ and MSN-MB-PEG in saline (300 μL) was administered to the tumor tissue by localized injection. Then, the tumor tissue was photoirradiated for 1 h. After irradiation, the mice were sacrificed and the tumor cells were harvested immediately for cell cycle analysis by flow cytometry. As shown in Figure 5, the cells obtained from the irradiated mice were arrested in G2/M phase, while those from the nonirradiated mice were not arrested. Thus, the present photoirradiation system is applicable to regulation of the cell cycle even in vivo.

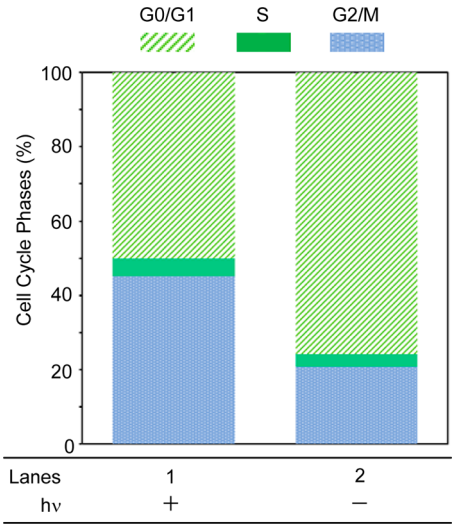

Figure 5. Cell cycle phases of colon 26 cells, which were collected from tumor tissue transplanted in mice. After the solution of preAQ (100 μM) and MSN-MB-PEG (10 mg/mL) in saline (300 μL) was administerd to the tumor tissue by localized injection, photoirradiation (665 nm) was conducted for 1 h. Then, the tumor cells were obtained immediately to analyze cell cycle phase by Nuclear-ID Green Cell Cycle Analysis kit for flow cytometry.

CONCLUSION

Two major problems of conventional methods for the regulation of cellular function by photoirradiation are the generation of ROS during photoirradiation and their low molecular selectivity in the chaotic environment of living cells. First, to achieve effective resolution of the problem that ROS strongly oxidize numerous biomolecules to damage living cells, we utilized the pores of nanoparticles as a constrained reaction field to produce confined $^1O_2$. Upon photoirradiation, MSN with photosensitizing MB units in their pore generated $^1O_2$ exclusively within the pores, which could not leak out from the pores due to its short lifetime. As a result, MSN-MB showed dramatically reduced photocytotoxicity, because the photochemical oxidation occurred predominantly in the pore. Second, we attempted to use the pores of MSN for selection of target molecules in the cells. The pore size successfully selected small molecules from large biomolecules such as nucleic acids or proteins, leading to selective photochemical conversion of the small molecules.

This newly designed intracellular photoreaction system was applied to photoregulation of the cell cycle. The cell cycle arrest reagent, AQ, was synthesized in living cells by the oxidation of the corresponding anthracene (preAQ) with singlet oxygen, leading to arrest of the cell cycle only after photoirradiation (Figure 4). Although the direct observation of intracellular AQ production was unsuccessful because the amount of AQ produced in the cells was small, it should be noted that we observed AQ production indirectly by checking the apoptotic pathway. We also confirmed that MSN-MB acted even in vivo for control of cellular functions in tumor tissue.

The present system, which can produce photochemical reactions in living cells without any side effects, offers new perspectives for the field of photochemistry. The applications of the system to photoregulation of single cell function and organelle-specific photoregulation by means of appropriate surface modification of MSN are in progress.

EXPERIMENTAL SECTION

General. All reagents were purchased from Nacalai Tesque (Kyoto, Japan), NOF Corporation (Tokyo, Japan), Life Technologies Japan (Tokyo, Japan), Wako pure Chemical Industries (Osaka, Japan), Tokyo Chemical Industry (Tokyo, Japan), or Sigma-Aldrich Japan (Tokyo, Japan), and were used without further purification. ^1H and ^{13}C NMR spectra were measured with a JEOL EX-400 or EX-300 spectrometer. Electrospray ionization mass spectrometry (ESI-MS) were conducted using a Thermo Fisher Scientific Exactive. Reversed phase high-performance liquid chromatography (RP-HPLC) was performed on a HITACHI D-2000 HPLC system using a Cosmosil 5C_8-MS column (5 μm, 4.6 × 250 mm) and the elution peaks were detected using a UV−vis detector L-7455 at 300 nm. The solvent mixture of 0.1 M triethylamine acetate (TEAA, pH 7.0) and acetonitrile was delivered as mobile phase at a flow rate of 0.6 mL/min at 40 °C. UV−vis NIR adsorption spectra were acquired on a JASCO V-530 spectrophotometer. Fluorescence spectra were recorded on a Shimadzu RF-5300PC spectrofluorophotometer. Transmission electron microscopy (TEM) images were taken on a JEOL JEM-1400 operated at 120 kV electron beam accelerating voltage. Zeta potentials of

DOI: 10.1021/acs.bioconjchem.6b00061
Bioconjugate Chem. XXXX, XXX, XXX−XXX

dispersed nanoparticles in water were measured with a Malvern Nano-ZS Zetasizer. Measurements were carried out in triplicate, and the Smoluchowski approximation was used to convert the electrophoretic mobility to zeta potential. Fluorescence data in living cells were recorded using a Promega GloMax Multi Detection System. MB-NH_2[39] was synthesized following a previously reported procedure. A confocal microscopy (Zeiss LSM710) was used for in vitro studies. Human lung carcinoma cell line, A549, was purchased from American Type Culture Collection (Manassas, VA) and colon 26 was given from Prof. Michiyuki Matsuda and Dr. Yuji Kamioka (Department of Medicine, Kyoto University). These cells were maintained in Dulbecco's Modified Eagle Medium (Invitrogen Corp., Carlsbad, CA) containing 10% of fetal bovine serum in a humidified incubator with 5% CO_2, 95% air at 37 °C. BALB/c nu/nu mice were purchased from SLC (Shizuoka, Japan). The mice were housed at the Institute of Laboratory Animals at Kyoto University Graduate School of Medicine. All studies and procedures were approved by Animal Research Committee of Kyoto University Graduate School of Medicine. All animal experiments were performed according to the Institutional Guidance of Kyoto University on Animal Experimentation and under permission of the animal experiment committee of Kyoto University.

Synthesis of N-(Anthraquinon-2-yl)-2-(dimethylamino)-acetamide (AQ). A mixture of 2-aminoanthraquinone (761 mg, 3.41 mmol), 2-chloroacetyl chloride (1.0 mL), and pyridine (0.8 mL) in DMF (1.0 mL) was stirred at r.t. for 18 h. The resulting mixture was added into a small amount of crushed ice, and the appearing precipitate was obtained by filtration. After washing with water, the residue was extracted with $CHCl_3$. Concentration of the resulting solution gave *N*-(anthraquinon-2-yl)-2-chloroacetamide as a brown solid. The chlorinated anthraquinone derivative was added into the mixture of 50% aqueous solution of dimethylamine (1.0 mL), pyridine (800 μL), and DMF (10 mL) without further purification and stirred at 80 °C for 3 h. The resulting mixture was quenched with water and then extracted with CH_2Cl_2. The obtained mixture was concentrated under reduced pressure and column chromatography (25−100% $CHCl_3$/Hexane) of the residue gave the desired product as a yellow powder (479 mg, 1.56 mmol, 46% over 2 steps): mp 141−143 °C; ^{1}H NMR (300 MHz, $CDCl_3$) δ 9.54 (br, 1H), 8.24 (dd, J = 8.8, 1.8 Hz, 1H), 8.16−8.13 (m, 3H), 8.02 (d, J = 1.8 Hz, 1H), 7.66 (t, J = 7.0 Hz, 2H), 3.08 (s, 2H), 2.36 (s, 6H); ^{13}C NMR (75 MHz, $CDCl_3$) δ 182.6, 181.7, 169.3, 143.0, 134.4, 134.0, 133.6, 133.4, 133.3, 129.0, 128.9, 127.0, 126.9, 123.8, 116.3, 63.4, 45.9; HR MS(ESI$^+$) m/z: Calcd for $C_{18}H_{17}N_2O_3^+$: 309.1234 $[M + H]^+$, found 309.1222 $[M + H]^+$.

Synthesis of N-(anthracen-2-yl)-2-(dimethylamino)-acetamide (preAQ). A mixture of 2-aminoanthracene (210 mg, 1.09 mmol), 2-chloroacetyl chloride (413 mg, 3.7 mmol), and triethylamine (120 μL) in dry THF (7.0 mL) was stirred at r.t. for 18 h. The resulting mixture was concentrated under reduced pressure and then extracted with ethyl acetate in the presence of water. Concentration of the resulting solution gave *N*-(anthracen-2-yl)-2-chloroacetamide as an orange−white solid. To a solution of the chlorinated anthraquinone derivative in dry THF (5 mL) was added dropwise 50% aqueous solution of dimethylamine (1.0 mL) and stirred at 50 °C for 3 h. The resulting mixture was concentrated under reduced pressure and column chromatography (0−16% MeOH/$CHCl_3$) of the residue gave the desired product as a bright yellow powder (145 mg, 0.52 mmol, 48% over 2 steps): mp 90−92 °C; ^{1}H NMR (400 MHz, $CDCl_3$) δ 9.28 (br, 1H), 8.45 (s, 1H), 8.32 (d, J = 10.2 Hz, 2H), 7.92 (d, J = 8.3 Hz, 3H), 7.46 (dd, J = 8.8, 2.0 Hz, 1H), 7.40 (m, 2H), 3.13 (s, 2H), 2.39 (s, 6H); ^{13}C NMR (100 MHz, $CDCl_3$) δ 169.0, 134.3, 132.1, 131.8, 131.0, 129.1, 129.1, 128.1, 127.8, 125.9, 125.5, 125.4, 124.8, 120.3, 115.0, 63.6, 45.9; HR MS(ESI$^+$) m/z: Calcd for $C_{18}H_{19}N_2O^+$: 279.1492 $[M + H]^+$, found 279.1484 $[M + H]^+$.

Surface Modification of Mesoporous Silica Nanoparticles (MSN). To a solution of MSN-CO_2H (1.0 mg) in DMSO (100 μL) was added a mixture of MB-NH_2 (595 μg, 1.1 μmol), EDCI (170 μg, 1.1 μmol), and DMAP (13 μg, 0.11 μmol) in DMSO (500 μL). The mixture was stirred at r.t. for 18 h. The blue precipitate was produced by the addition of water (500 μL) and isolated by centrifuging at 13.2k rpm for 10 min. Washing of this precipitate with water three times gave MSN-MB as a dark blue powder. MSN-anth is also fabricated following the above method from carboxylic-functionalized MSN, an excess of 2-aminoanthracene and condensation agents.

Synthesis of MSN-MB-PEG.[40] To a solution of MSN-CO_2H (165 mg, 6.8 μmol of COOH units) in DMF (10 mL) were added PEG-NH_2 [MW 42 000] (10.3 mg, 0.24 μmol, 3.5% equiv, ME-400EA from NOF corporation), *N*,*N*-dicyclohexylcarbodiimide (DCC) (2.1 mg, 10 μmol), and DMAP (0.5 mg, 4.1 μmol). The reaction mixture was stirred at room temperature for 18 h, and the resulting solutions was centrifuged at 1500 rpm for 3 min in 15 mL tube to remove the supernatant. Further washing with DMSO and water afforded MSN with both PEG units and CO_2H units (MSN-CO_2H-PEG) as a white powder. This highly hydrosoluble nanoparticles was subsequently mixed with MB-NH_2 (6 μmol) in DMSO (5 mL) including EDCI (1.7 mg, 10.1 μmol) and DMAP (0.2 mg, 1.6 μmol) at r.t. for 18 h. Water (3 mL) was added to the resulting mixture and a blue precipitate was produced. To isolate the blue precipitate, the mixture was centrifuged at 3 krpm for 5 min and washed with water twice. Drying under reduced pressure afforded MSN-MB-PEG as a bright blue powder (54 mg). The formation of MSN-MB-PEG was identified by measurement of UV spectra (see Figure S4).

Cell Culture. The cells were cultured at 37 °C in 5% CO_2 in 75 cm^2 flasks containing Dulbecco's Modified Eagle Medium (D-MEM) supplemented with 10% fetal bovine serum (FBS) and 1% antibiotics.

Fluorescence Microscope Imaging. For fluorescence imaging, the cells were plated in an imaging microplate (μ-Dish 35 mm) with a seeding density of 5×10^4 cells per well, and preincubated for 24 h. The cells were further incubated for 3 h with either MSN-MB (1.0 mg/mL) or MB-NH_2 (41 μM) in 300 μL D-MEM. After washing with the medium (no Phenol Red), the cells were observed with a confocal laser scanning microscopy (Zeiss, LSM710) using appropriate excitation and emission filters.

Cytotoxicity Assay (WST-8 Assay). The cytotoxicity assays were performed in 96-well plates with a seeding density of 1×10^4 cells per well. The cells were preincubated overnight at 37 °C in 5% CO_2 and then further incubated for 24 h with the medium containing test substances. After incubation, 10 μL of Cell Counting Kit-8 solution (Dojindo) was added to each well and the plates were incubated for 3 h at 37 °C in 5% CO_2. Absorbance at 450 nm was recorded on a xMark microplate spectrophotometer (BioRad).

DOI: 10.1021/acs.bioconjchem.6b00061
Bioconjugate Chem. XXXX, XXX, XXX−XXX

Quantification of Generated Singlet Oxygen in Cells. Generated singlet oxygen was measured by using Singlet Oxygen Sensor Green (SOSG) containing a fluorescein unit. Cells were plated in 96-well plates with a seeding density of 1×10^4 cells per well for 24 h and then incubated in the presence or absence of MSN-MB (0.1 mg, 4.1 nmol MB units) in 100 μL D-MEM including SOSG (25 μM) for 5 h. After washing with D-MEM (no phenol red) three times, the cells were irradiated by visible light (665 nm, 2.0 mW/cm^2) for 0 or 1 h, and then the fluorescence intensity of the cells was recorded on a fluorescence plate reader (Promega GloMax Multi Detection System) (Ex/Em: 490/510−570 nm).

Determination of GSH/GSSG Ratio. Levels of GSH and GSSG were measured using a GSH/GSSG quantification kit (Dojindo, Japan). Briefly, A549 cells were preincubated overnight at 37 °C in 5% CO_2 and further incubated for 24 h with the medium containing test substances. After washing with DPBS three times, the cells were irradiated by visible light (665 nm, 2.0 mW/cm^2) for 30 min. The cells were harvested and centrifuged for 10 min and the supernatant discarded. The pellets were washed with 500 μL of cold DPBS and centrifuged for 10 min at 4 °C and the supernatant discarded. After the pellets were resuspended with 80 μL of 10 mM HCl, the cell suspensions were frozen−thawed twice. Then, 20 μL of 5% 5-sulfosalicylic acid (SSA) was added to the suspensions and centrifuged for 10 min at 4 °C. The supernatants were diluted with ultrapure water to reduce the SSA concentration to 0.5% for assay. The samples were reacted with 5-mercapto-2-nitrobenzoic acid and the absorbance at 405 nm was recorded on a xMark microplate spectrophotometer.

Active Area of Singlet Oxygen. Active singlet oxygen was determined by using the fluorescence property of anthracene tethered in the pore of MSN (MSN-Anth). MSN-Anth (0.2 mg) was stirred with either MSN-MB (0.1 mg, 4.1 nmol) or MB-NH_2 (4.1 nmol) in DMSO (1 mL) upon photoirradiation (665 nm, 2.0 mW/cm^2) for 0, 1, 2, 3, 5, 10, and 20 min. The fluorescence intensities of the resulting samples were measured on a Shimadzu RF-5300PC spectrofluorophotometer and plotted (Ex/Em: 380/535 nm).

Generation of AQ from preAQ. After bubbling 100% oxygen gas through a solution of preAQ (1 mM) and MB (41 μM) in water (1 mL) for 30 min, the solution was exposed to visible light (665 nm, 2.0 mW/cm^2) for 0, 1, 2, and 3 h. The irradiated solutions (20 μL) were analyzed using reversed phase HPLC. The detection wavelength was 300 nm and the retention time of preAQ and AQ were 38.6 and 32.2 min, respectively. After purification by HPLC, the formation of AQ was identified by ESI-MS; HR MS(ESI$^-$) m/z: Calcd for $C_{18}H_{15}N_2O_3^-$: 307.1088 $[M-H]^-$, found 307.1091 $[M-H]^-$.

Cell Cycle Analyses on a Flow Cytometer. Cell cycle analyses were performed following the instruction manual of Nuclear-ID Green Cell Cycle Analysis Kit for Flow Cytometry (Enzo Life Sciences). Cells were plated in 12-well plates with a seeding density of 5×10^4 cells per well and then treated with each reagent (10 μM) and/or MSN-MB (1.0 mg/mL) and/or NaN_3 (100 μM) in D-MEM (1 mL) for 24 h. After washing with D-MEM (no phenol red) three times, the cells were irradiated by visible light (665 nm) for 6 h and further incubated for 24 h. The prepared adherent cells ($\sim 1 \times 10^5$ cells) were trypsinized and centrifuged at 1000 rpm for 5 min to remove the supernatant. The isolated cells were resuspended in 0.5 mL of freshly prepared DNA Staining Solution, incubated at 37 °C for 30 min in the dark, and then analyzed in FITC channel of a flow cytometer with a 488 nm excitation laser and a 530 nm detection filter. The obtained profiles were analyzed in a Flowjo software (Tree Star) by Dean-Jett-Fox fitting curve model.

Determination of Active Caspase 3 and 9. The ratio of active caspase 9 to active caspase 3 was examined by immunofluorescence detection with APO Logix caspase detection kit (Cell Technology). Cell treatment by AQ (10 μM), MSN-MB (1.0 mg/mL, 41 μM MB), preAQ (10 μM), or methylene blue (41 μM) were incubated for 24 h. After washing of the cells, photoirradiation (665 nm, 2.0 mW/cm^2) was conducted for 3 h. All samples were further incubated for 72 h and the cell cycles were analyzed by detection kit.

Cell Cycle Photoregulation in Vivo. For the cell cycle photoregulation in vivo, tumor bearing mice were subcutaneously injected MSN-MB-PEG (10 mg/mL) and preAQ (100 μM) in saline (300 μL). After 24 h, the mice were irradiated (665 nm, 2.0 mW/cm^2) for 1 h. Then, the mice were sacrificed and the resected tumor cells were immediately dispersed by the usual collagenase treatment. To analyze the cell cycle, the obtained tumor cells were treated with Nuclear ID detection kit and measured by using a flow cytometer as mentioned above.

Calculation of Inner and Outer Area of MSN Surface. Inner and outer MSN surface area were calculated by eq 1 and eq 2, respectively. Assuming that MSN (radius: 100 nm) is composed of tubes (radius: 1.75 nm) hexagonally arranged in 28 layers ($\sim$100/3.5) from the center, the inner and outer areas were expressed in the following equations

$$\text{Inner area} = 1 \times 2\pi r \times 2\sqrt{R^2 - \left(r\left(1 - \frac{1}{2}\right)\right)^2} + \sum_{n=2}^{28} (6(n-1)) \times 2\pi r \times 2\sqrt{R^2 - \left(r\left(n - \frac{1}{2}\right)\right)^2} \quad (1)$$

$$\text{Outer area} = 4\pi R^2 \quad (2)$$

where R = MSN radius (= 100 nm) and r = the pore radius (= 1.75 nm). Consequently, the inner area and outer area are 3.4×10^6 nm^2 and 1.3×10^5 nm^2 per particle, respectively. Therefore, the ratio of the inner area to the total area is approximately 96%.

■ ASSOCIATED CONTENT

Supporting Information

The Supporting Information is available free of charge on the ACS Publications website at DOI: 10.1021/acs.bioconjchem.6b00061.

Additional experimental results for characterization of MSN-MB in the cells and photoreaction of preAQ, and synthesis of MSN-MB-PEG (PDF)

■ AUTHOR INFORMATION

Corresponding Author

*Phone: +81-42-759-6229. FAX: +81-42-759-6493. E-mail: tanabe.kazuhito@chem.aoyama.ac.jp.

Notes

The authors declare no competing financial interest.

DOI: 10.1021/acs.bioconjchem.6b00061
Bioconjugate Chem. XXXX, XXX, XXX−XXX

■ ACKNOWLEDGMENTS

We sincerely thank Professor Teruyuki Kondo (Kyoto University) for his valuable discussions and supports during this study. We also thank Professor Tadashi Suzuki (Aoyama Gakuin University) for valuable discussions about physical−chemical properties of the compounds. This work is partly supported by the Innovative Techno-Hub for Integrated Medical Bioimaging Project of the Special Coordination Funds for Promoting Science and Technology, and by Grant-in-Aid for Scientific Research, from the Ministry of Education, Culture, Sports, Science and Technology (MEXT), Japan.

■ REFERENCES

(1) Halloran, M. C., Sato-Maeda, M., Warren, J. T., Su, F., Jr., Lele, Z., Krone, P. H., Kuwada, J. Y., and Shoji, W. (2000) Laser-induced gene expression in specific cells of transgenic zebrafish. *Development 127*, 1953−1960.

(2) Kamei, Y., Suzuki, M., Watanabe, K., Fujimori, K., Kawasaki, T., Deguchi, T., Yoneda, Y., Todo, T., Takagi, S., Funatsu, T., et al. (2009) Infrared laser-mediated gene induction in targeted single cells in vivo. *Nat. Methods 6*, 79−81.

(3) Wang, Y., He, H., Li, S., Liu, D., Lan, B., Hu, M., Cao, Y., and Wang, C. (2014) All-optical regulation of gene expression in targeted cells. *Sci. Rep. 4*, 5346−5351.

(4) Yamazoe, S., Liu, Q., McQuade, L. E., Deiters, A., and Chen, J. K. (2014) Sequential gene silencing using wavelength-selective caged morpholino oligonucleotides. *Angew. Chem., Int. Ed. 53*, 10114−10118.

(5) Miyako, E., Deguchi, T., Nakajima, Y., Yudasaka, M., Hagihara, Y., Horie, M., Shichiri, M., Higuchi, Y., Yamashita, F., Hashida, M., et al. (2012) Photothermic regulation of gene expression triggered by laser-induced carbon nanohorns. *Proc. Natl. Acad. Sci. U. S. A. 109*, 7523−7528.

(6) Miyako, E., Russier, J., Mauro, M., Cebrian, C., Yawo, H., Menard-Moyon, C., Hutchison, J. A., Nakajima, Y., Yudasaka, M., Iijima, S., et al. (2014) Photofunctional nanomodulators for bioexcitation. *Angew. Chem., Int. Ed. 53*, 13121−13125.

(7) Stanley, S. A., Gagner, J. E., Damanpour, S., Yoshida, M., Dordick, J. S., and Friedman, J. M. (2012) Radio-wave heating of iron oxide nanoparticles can regulate plasma glucose in mice. *Science 336*, 604−608.

(8) Yazawa, M., Sadaghiani, A. M., Hsueh, B., and Dolmetsch, R. E. (2009) Induction of protein-protein interactions in live cells using light. *Nat. Biotechnol. 27*, 941−945.

(9) Bugaj, L. J., Choksi, A. T., Mesuda, C. K., Kane, R. S., and Schaffer, D. V. (2013) Optogenetic protein clustering and signaling activation in mammalian cells. *Nat. Methods 10*, 249−252.

(10) Piette, J. (1990) Mutagenic and genotoxic properties of singlet oxygen. *J. Photochem. Photobiol., B 4*, 335−339.

(11) Davies, M. J. (2003) Singlet oxygen-mediated damage to proteins and its consequences. *Biochem. Biophys. Res. Commun. 305*, 761−770.

(12) Cadet, J., Ravanat, J. L., Martinez, G. R., Medeiros, M. H., and Di Mascio, P. (2006) Singlet oxygen oxidation of isolated and cellular DNA: product formation and mechanistic insights. *Photochem. Photobiol. 82*, 1219.

(13) Klotz, L. O., Kroncke, K. D., and Sies, H. (2003) Singlet oxygen-induced signaling effects in mammalian cells. *Photochem. Photobiol. Sci. 2*, 88−94.

(14) Qian, X., Fuku, K., Kuwahara, Y., Kamegawa, T., Mori, K., and Yamashita, H. (2014) Design and functionalization of photocatalytic systems within mesoporous silica. *ChemSusChem 7*, 1528−1536.

(15) Thomas, J. M., and Sankar, G. (2001) The role of synchrotron-based Studies in the elucidation and design of active sites in titanium−silica epoxidation catalysts. *Acc. Chem. Res. 34*, 571−581.

(16) Noji, T., Kondo, M., Jin, T., Yazawa, T., Osuka, H., Higuchi, Y., Nango, M., Itoh, S., and Dewa, T. (2014) Light-driven hydrogen production by hydrogenases and a Ru-complex inside a nanoporous glass plate under aerobic external conditions. *J. Phys. Chem. Lett. 5*, 2402−2407.

(17) Yamamoto, Y., Takeda, H., Yui, T., Ueda, Y., Koike, K., Inagaki, S., and Ishitani, O. (2014) Efficient light harvesting via sequential two-step energy accumulation using a Ru-Re_5 multinuclear complex incorporated into periodic mesoporous organosilica. *Chem. Sci. 5*, 639−648.

(18) Vallet-Regi, M., Rámila, A., del Real, R. P., and Pérez-Pariente, J. (2001) A new property of MCM-41: Drug Delivery System. *Chem. Mater. 13*, 308−311.

(19) Tang, F., Li, L., and Chen, D. (2012) Mesoporous silica nanoparticles: synthesis biocompatibility and drug delivery. *Adv. Mater. 24*, 1504−1534.

(20) Mondragon, L., Mas, N., Ferragud, V., de la Torre, C., Agostini, A., Martinez-Manez, R., Sancenon, F., Amoros, P., Perez-Paya, E., and Orzaez, M. (2014) Enzyme-responsive intracelular-controlled release using silica mesoporous nanoparticles capped with ϵ−poly-$_L$-lysine. *Chem. - Eur. J. 20*, 5271−5281.

(21) Frasconi, M., Liu, Z., Lei, J., Wu, Y., Strekalova, E., Malin, D., Ambrogio, M. W., Chen, X., Botros, Y. Y., Cryns, V. L., et al. (2013) Photoexpulsion of surface-grafted ruthenium complexes and subsequent release of cytotoxic cargos to cancer cells from mesoporous silica nanoparticles. *J. Am. Chem. Soc. 135*, 11603−11613.

(22) Cheng, S. − H., Lee, C. − H., Yang, C. − S., Tseng, F. − G., Mou, C.-Y., and Lo, L. − W. (2009) Mesoporous silica nanoparticles functionalized with an oxygen-sensing probe for cell photodynamic therapy: potential cancer theranostics. *J. Mater. Chem. 19*, 1252−1257.

(23) Ranby, B., Rabek, J. F. (1978) *Singlet oxygen reactions with organic compounds and polymers*, John Wiley and Sons Ltd., London.

(24) Moan, J. (1990) On the diffusion length of singlet oxygen in cells and tissues. *J. Photochem. Photobiol., B 6*, 343−347.

(25) Wilkinson, F., Helman, W. P., and Ross, A. B. (1995) Rate constants for the decay and reactions of the lowest electronically. Excited singlet state of molecular oxygen in solution. *J. Phys. Chem. Ref. Data 24*, 663−1021.

(26) Tanaka, K., Miura, T., Umezawa, N., Urano, Y., Kikuchi, K., Higuchi, T., and Nagano, T. (2001) Rational design of fluorescein-based fluorescence probes. Mechanism-based design of a maximum fluorescence probe for singlet oxygen. *J. Am. Chem. Soc. 123*, 2530−2536.

(27) Kim, S., Tachikawa, T., Fujitsuka, M., and Majima, T. (2014) Far-red fluorescence probe for monitoring singlet oxygen during photodynamic therapy. *J. Am. Chem. Soc. 136*, 11707−11715.

(28) Hsin, L. − W., Wang, H. − P., Kao, P. − H., Lee, O., Chen, W. − R., Chen, H. − W., Guh, J. − H., Chan, Y. − L., His, C. − P., Yang, M. − S., et al. (2008) Synthesis, DNA binding, and cytotoxity of 1,4-bis(2-amino-ethylamino)anthraquinone-amino acid conjugates. *Bioorg. Med. Chem. 16*, 1006−1014.

(29) Katzhendler, J., Gean, K. − F., Bar-Ad, G., Tashma, Z., Ben-Shoshan, R., Ringel, I., Bachrach, U., and Ramu, A. (1989) Synthesis of aminoanthraquinone derivatives and their in vitro evaluation as potential anti-cancer drugs. *Eur. J. Med. Chem. 24*, 23−30.

(30) Agbandje, M., Jenkins, T. C., McKenna, R., Reszka, A. P., and Neidle, S. (1992) Anthracene-9,l0-diones as potential anticancer agents. Synthesis, DNA-binding, and biological studies on a series of 2,6-disubstituted derivatives. *J. Med. Chem. 35*, 1418−1429.

(31) Tu, H. − Y., Huang, A. − M., Teng, C. − H., Hour, T. − C., Yang, S. − C., Pu, Y. − S., and Lin, C. − N. (2011) Anthraquinone derivatives induce G2/M cell cycle arrest and apoptosis in NTUB1 cells. *Bioorg. Med. Chem. 19*, 5670−5678.

(32) Zeng, G. − Z., Fan, J. − T., Xu, J. − J., Li, Y., and Tan, N. − H. (2013) Apoptosis induction and G2/M arrest of 2-methyl-1,3,6-trihydroxy-9,10-anthraquinone from *Rubia yunnanensis* in human cervical cancer HeLa cells. *Pharmazie 68*, 293−299.

(33) Srinivas, N., Radha Rani, V., Kulkarni, S. J., and Raghavan, K. V. (2002) Liquid phase oxidation of anthracene and trans-stilbene over modified mesoporous (MCM-41) molecular sieves. *J. Mol. Catal. A: Chem. 179*, 221−231.

DOI: 10.1021/acs.bioconjchem.6b00061
Bioconjugate Chem. XXXX, XXX, XXX−XXX

(34) Fukuzumi, S., and Ohkubo, K. (2013) Selective photocatalytic reactions with organic photocatalysts. *Chem. Sci. 4*, 561−574.
(35) Cui, Q., Yu, J. − H., Wu, J. − N., Tashiro, S., Onodera, S., Minami, M., and Ikejima, T. (2007) P53-mediated cell cycle arrest and apoptosis through a caspase-3-independent, but caspase-9-dependent pathway in oridonin-treated MCF-7 human breast cancer cells. *Acta Pharmacol. Sin. 28*, 1057−1066.
(36) Zhuang, S., Lynch, M. C., and Kochevar, I. E. (1999) Caspase-8 mediates caspase-3 activation and cytochrome c release during singlet oxygen-induced apoptosis of HL-60 cells. *Exp. Cell Res. 250*, 203−212.
(37) Foo, J. B., Yazan, L. S., Armania, N., Ismail, N., Imam, M. U., Yeap, S. K., Cheah, Y. K., Abdullah, R., and Ismail, M. (2014) Induction of cell cycle arrest and apoptosis in caspase-3 deficient MCF-7 cells by Dillenia suffruticosa root extract via multiple signalling pathways. *BMC Complementary Altern. Med. 14*, 197−212.
(38) Zhuang, S., Demirs, J. T., and Kochevar, I. E. (2000) p38 Mitogen-activated protein kinase mediates bid cleavage, mitochondrial dysfunction, and caspase-3 activation during apoptosis induced by singlet oxygen but not by hydrogen peroxide. *J. Biol. Chem. 275*, 25939−25948.
(39) New, O. M., and Dolphin, D. (2009) Design and synthesis of novel phenothiazinium photosensitizer derivatives. *Eur. J. Org. Chem. 2009*, 2675−2686.
(40) Kim, M. S., Jeon, J. B., and Chang, J. Y. (2013) Selectively functionalized mesoporous silica particles with the PEGylated outer surface and the doxorubicin-grafted inner surface: Improvement of loading content and solubility. *Microporous Mesoporous Mater. 172*, 118−124.

DOI: 10.1021/acs.bioconjchem.6b00061
Bioconjugate Chem. XXXX, XXX, XXX−XXX